Geochimica et Cosmochimica Acta, Vol. 69, No. 6, pp. 1413–1422, 2005

0016-7037/05 $30.00 + .00

doi:10.1016/j.gca.2004.09.008

TEM study of a silicate–carbonate–microbe interface prepared by focused ion beam milling

KARIM BENZERARA,[†,1,*] NICOLAS MENGUY,[2,†] FRANÇOIS GUYOT[2], CHRISTIAN VANNI[3], and PHILIPPE GILLET[4]

[1]Surface & Aqueous Geochemistry Group, Department of Geological and Environmental Sciences, Stanford University, Stanford, CA 94305-2115, USA

[2]Laboratoire de Minéralogie-Cristallographie, UMR 7590 CNRS and Institut de Physique du Globe de Paris, 4 place Jussieu, 75252 Paris Cedex, France

[3]Laboratoire CP2M Faculté des Sciences et Techniques de Saint Jerôme, Université d'Aix-Marseille, III, F-13397 Marseille Cedex 20, France

[4]Laboratoire des Sciences de la Terre, Ecole Normale Supérieure Lyon. 46 Allée d'Italie, 69007 Lyon Cedex, France

(Received April 27, 2004; accepted in revised form September 14, 2004)

Abstract—The biogeochemical alteration of an Mg-Fe orthopyroxene, reacted for 70 yr under arid conditions in a desert environment, was studied by transmission electron microscopy. For this purpose, an electron transparent cross-section of the interface between a single microorganism, an orthopyroxene and nanometer-sized calcite crystals, was prepared with a focused ion beam system. X-ray energy dispersive spectrometry and electron energy loss spectroscopy allowed one to clearly distinguish the microorganism en route to fossilization from the nanometer-sized calcite crystals, showing the usefulness of such a protocol for identifying unambiguously traces of life in rocks. A 100-nm-deep depression was observed in the orthopyroxene close to the microorganism, suggesting an enhanced dissolution mediated by the microbe. However, an Al- and Si-rich amorphous altered layer restricted to the area just below the microorganism could be associated with decreased silicate dissolution rates at this location, suggesting complex effects of the microorganism on the silicate dissolution process. The close association observed between silicate dissolution and carbonate formation at the micrometer scale suggests that Urey-type CO_2 sequestration reactions could be mediated by microorganisms under arid conditions.

1. INTRODUCTION

The weathering of pyroxene can release Fe, Mg, Ca, Al, and Si as well as trace metals, which are essential nutrients for microbial and plant growth. Understanding which parameters control this reaction is also important, because the alteration of Ca- and Mg-containing silicates buffers the level of atmospheric CO_2 at the geological scale (Berner, 1995). Indeed, silicate weathering withdraws CO_2 from the atmosphere ultimately trapped in carbonate minerals, which precipitate in the oceans (Urey, 1952). Abiotic dissolution of enstatite (pure Mg pyroxene) is now accurately modeled in the 1–11 pH range at 25°C (Oelkers and Schott, 2001; see also Brantley and Chen, 1995 for a review). The presence of Fe adds complexity to the system. Schott and Berner (1983) showed that, under oxic conditions and at neutral pH, an iron oxide layer and a Fe^{3+} hydroxylated silicate layer, resulting from oxidation of iron from pyroxene could inhibit the dissolution after some time. The existence of armoring surface layers formed during the alteration of silicates, which have a huge impact on the effective dissolution rates of these minerals, has been a matter of intense debate. The formation of altered surface layers was observed in dissolution experiments of silicates (Casey et al., 1989a; Casey et al., 1993; Banfield et al., 1995; Hellmann et al., 2003; Benzerara et al., 2004) and on naturally weathered feldspars (Nesbitt and Muir, 1988; Nugent et al., 1998). Amorphous layers have almost never been clearly detected, however, on naturally weathered pyroxene surfaces (Nahon and Colin, 1982; Brantley and Chen, 1995).

It has been postulated and observed that microorganisms could have a major effect on the weathering rates of silicates via the production of organic ligands or by promoting Fe redox reactions (for a review, Barker et al., 1997). However, only few studies have investigated the interface between silicates and microorganisms at the scale at which the reactions occur, i.e., the nanometer scale. Barker and Banfield (1996) were precursors by cross-sectioning micrometer-sized lichen-colonized amphiboles by ultramicrotomy and by studying the interface by high-resolution transmission electron microscopy (HRTEM). Despite the importance of such a study, it has not been reproduced for other samples from different environments or different mineral compositions, which could have given a broader view on the variety of microbes–silicates interactions in nature. One possible reason is that the use of transmission electron microscopy (TEM) has been hindered up to now by the inaccuracy of the sample preparation techniques. Classical procedures include (1) crushing of the sample in ethanol or water, (2) ion milling, and (3) ultramicrotomy. Ultramicrotomy is the only one of these three techniques which can preserve the contacts between the organic and mineral counterparts, but it is restricted to samples with micrometer-sized minerals and does not offer the possibility to select the sampled area with a high spatial specificity. This prevents using it in low biomass samples, in which the area of interest is restricted to few micrometers if not to a single microbial cell.

Benzerara et al. (2003) have shown that the Tatahouine meteorite is a pertinent object for studying the weathering of Fe-Mg pyroxene by microorganisms under arid conditions.

* Author to whom correspondence should be addressed (benzerar@stanford.edu).

† Equal contribution from the first two co-authors.

Some fragments of this meteorite, which is almost exclusively composed of orthopyroxene (Barrat et al., 1998), were collected the day after its fall in arid south Tunisia in 1931 (Lacroix, 1932). New fragments were then collected in the Tatahouine sand 70 yr after the fall (Benzerara et al., 2003). The comparison between two sets of samples thus allows unraveling the effects of terrestrial microbial colonization on the pyroxene geochemistry. With scanning electron microscopy (SEM), Benzerara et al. (2003) observed a spatial correlation between a microbial filament, nanometer-sized rod-shaped calcite crystals, and a possible alteration of the underlying pyroxene, but the interactions between those three components could not be described more precisely on the basis of these observations. In this study we have used the focused ion beam (FIB) technique to prepare ultrathin cross-sections for TEM with a less than 100-nm positional accuracy, offering great promise for the study of microbial–mineral interactions. The subsequent observations by TEM (combining high-resolution observations and spectroscopic analyses) offer the capacity to scrutinize, at the nanometer scale, the geochemical processes occurring at the interface between a microorganism, calcite precipitates, and a Fe-Mg pyroxene.

2. EXPERIMENTAL METHODS

2.1. SEM Observations and Energy Dispersive X-ray Spectrometry (EDXS) Maps

The gold-coated meteorite fragments collected in 2000 and described in Benzerara et al. (2003) were reobserved by SEM. Operating conditions of the Philips XL30 S FEG-SEM (FEG: Field Emission Gun) were 5 kV accelerating voltage with a working distance of 5 to 15 mm. For EDXS chemical analyses, an acceleration voltage of 20 kV was used.

2.2. Cross-Sectioning by the FIB Technique

FIB milling was performed with a FEI Model 200 TEM FIB system at the University Aix-Marseille III. The FIB lift-out method was used to prepare the sample (Fig. 1b) as described in Heaney et al. (2001). The same area as that observed by SEM could be easily located using the imaging capabilities of the FIB. A thin layer of platinum was then deposited on the specimen across the filament and the calcite cluster (Fig. 1a) to protect them during the milling process. The FIB system uses a Ga liquid metal ion source which allows milling. A 30-kV Ga^+ beam operating at ~20 nA excavated pyroxene from both sides of the Pt layer to a depth of 5 μm, resulting in the achievement of a thin cross-section. Before removal of the thin slide, the sample was further thinned to ~80 nm with a glancing angle beam at much lower beam currents of ~100 pA. Finally, a line pattern was drawn with the ion beam along the side and bottom edges of the thin section, allowing its removal. The ~ 15 μm × 5 μm × 80 nm slide was transferred at room pressure with the aid of a stereomicroscope and a hydraulic micromanipulator. A glass needle was directed to the thin slide which was extracted by electrostatic attraction to the needle. The cross-section was then deposited onto the membrane of a carbon-coated 200-mesh copper grid. The obtained foil, whose thickness is estimated to 80 nm, e.g., electron transparent, is shown in Figure 1c.

2.3. TEM, EDXS, and Electron Energy Loss Spectroscopy (EELS) Analyses

TEM observations were carried out on a Jeol 2010F microscope operating at 200 kV, equipped with a field emission gun, a high-resolution Ultra High Radiation (UHR) pole piece, and a Gatan energy filter GIF 200. EDXS analyses were performed using a Kevex detector with an ultrathin window allowing detection of light elements. Analyses were recorded with typical total counts of 40,000. EELS spectra were acquired using a dispersion of 0.3 eV/channel to record spectra in the range 250 eV to 560 eV. The energy resolution was ~1.3 eV as measured by the full width at half maximum of the zero-loss peak. The dwell time was optimized to acquire sufficient signal intensity and to limit beam damage. Spectra were corrected from plural scattering using the Egerton procedure available with the EL/P program (Gatan).

3. RESULTS

3.1. SEM Observation of the Sample

SEM was used to locate the area depicted in Benzerara et al. (2003), and chemical mapping was processed with EDXS (Fig. 2). Figure 2a shows a 1 μm × 25 μm flat filament. The filament's edges are outlined on the carbon map, indicating that carbon is associated with the filament (Fig. 2b). A carbon- and calcium-rich area is observed on the right-hand side of the filament (Fig. 2). This area corresponds to a cluster of rod-shaped calcite single crystals (Benzerara et al., 2003). We used FIB milling to prepare an ultrathin cross-section for TEM across the interface between the long flat filament, the calcite nanocrystals cluster, and the underlying meteorite (see location on Fig. 2a).

3.2. Chemistry of the Calcite Crystals and of the Flat Filament

The different components of interest (organic filament, calcite nanocrystals, and orthopyroxene) are clearly recognized by TEM and are located at the same place as that shown by SEM (Fig. 1c). EDXS and EELS analyses were performed on the calcite crystals and on the putative microorganism (i.e., the long flat filament) as shown in Figure 3. By recording blank spectra on the sample-free film adjacent to areas of interest, the contribution from the formvar film to the analyses presented here was shown to be negligible except for EELS analyses at the C-K edge. EDXS analyses of calcite crystals (Fig. 3a) are consistent with a low-magnesium and low-iron calcite composition as previously reported (Benzerara et al., 2003). Small iron and magnesium peaks could, however, be evidenced in the EDXS spectra for several crystals. The EELS C-K-edge spectra are similar for several nanocrystals and show two main peaks at 290.5 eV and 301 eV (Fig. 3b), which are unambiguously indicative of the carbonate group (Hofer and Golob, 1987). A small peak at 286 eV could be detected and cannot be assigned to carbonate. Similarly, O-K edge EELS spectroscopy reveals the presence of a peak at 532 eV that is not related to the carbonate bond (Fig. 3c).

EDXS analyses performed on the flat filament confirm the high carbon and oxygen content of this object (Fig. 3d), and the presence of phosphorus (Fig. 3e). EELS spectra on the flat filament showed a peak at 402 eV corresponding to the nitrogen K-edge (Fig. 3f). The carbon K-edge spectra in the filament are notably different from that measured on the nano-calcite crystals (insert in Fig. 3f) and are typical of an amorphous, likely organic, carbon (Mansot et al., 2003). These data strongly support the biologic nature of this filament. The presence of silicon, iron, and calcium in the microorganism was shown by EDXS or EELS, or both. Neither crystallized carbonates nor crystallized iron oxide phases could, however, be evidenced by high-resolution imaging.

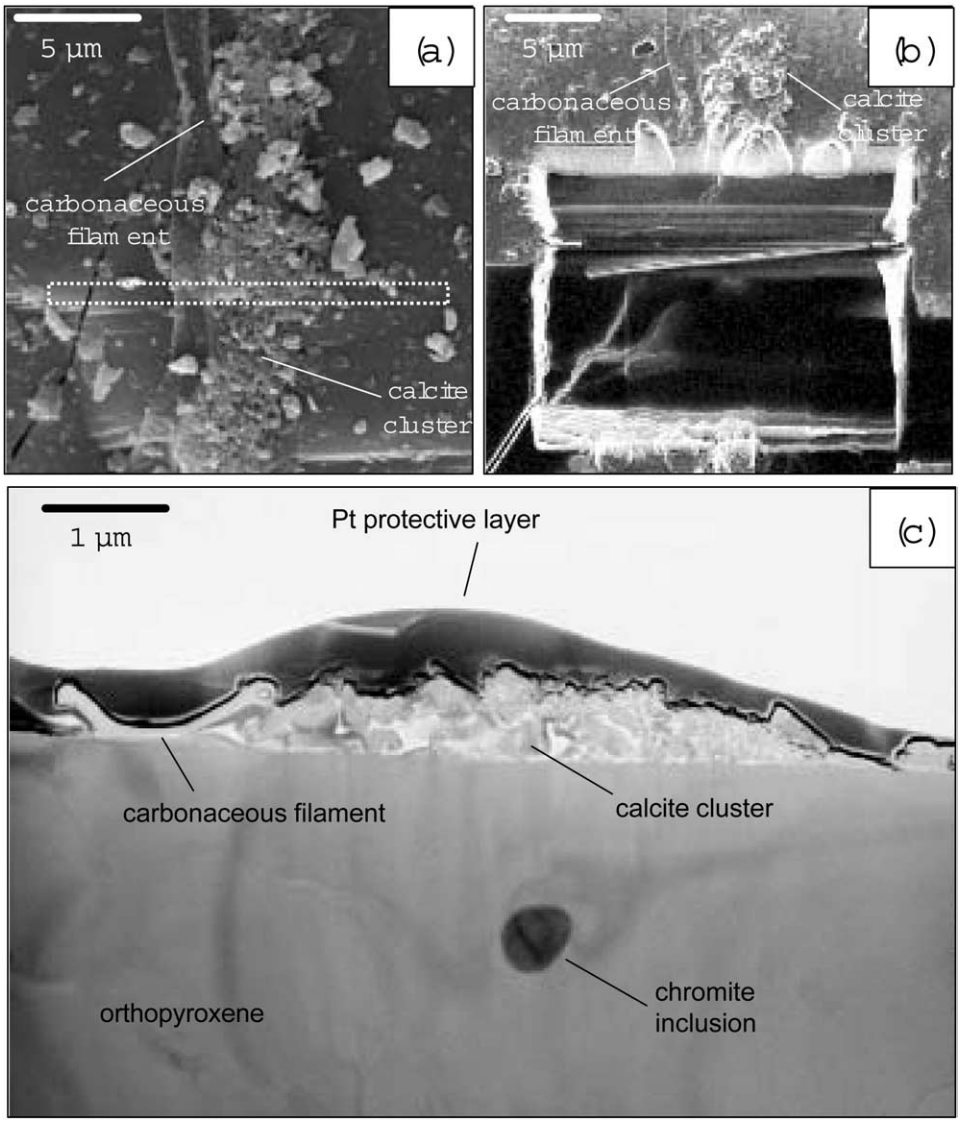

Fig. 1. Focused ion beam (FIB) cross-sectioning of the filament, the calcite cluster, and the pyroxene. (a) FIB image of the sampled area before the cross-sectioning. The dotted rectangle indicates the position where the platinum layer is deposited. The positional accuracy is better than 100 nm. (b) FIB image of the ultrathin section still in place before the micromanipulator-assisted extraction stage. (c) TEM images of the cross-section showing the platinum (Pt) protective layer, the flat carbonaceous filament (left), the calcite cluster, the orthopyroxene, and a chromite inclusion.

3.3. High-Resolution Study of the Pyroxene Surface

EDXS analyses of the underlying mineral were consistent with the composition of the bronzite $(Mg_{0.75}Fe_{0.23}Ca_{0.01})(Si_{0.99}Al_{0.01})O_3$, which composes almost exclusively the Tatahouine meteorite (Barrat et al., 1999). At low magnification, whereas the pyroxene surface appeared flat on both far sides of the cross-section, we evidenced a 100-nm-deep depression centered on the calcite cluster (Fig. 4a). A smaller depression could be observed just below the microorganism. High-resolution images showed that the pyroxene surface was rougher below the microbe as compared to adjacent areas on the pyroxene surface (Fig. 4b), including the regions below the calcite cluster. The interface between the microbial filament and the underlying pyroxene was observed at a slight defocus to enhance the contrast of noncoherently diffracting objects (Fig. 5). A fibrous layer was detected in this way between the microorganism and the pyroxene surface (Fig. 5a). Selected area diffraction pattern and high-resolution observations showed that this layer is mostly amorphous or ill-crystallized (Fig. 5b). Moreover, EDXS analyses showed that this region has a similar composition as the orthopyroxene but contains less magnesium, a significantly higher aluminum content, and some potassium (Fig. 5e and 5d). It is noteworthy that no amorphous layer could be detected below the calcite clusters. One nanometer-sized rod-shaped crystal lying at the pyroxene surface could be observed in the amorphous layer (Fig. 5f). EDXS and Fast Fourier trans-

form (FFT) of high-resolution images of this particle are consistent with a clay mineral (illite- or smectite-like). FFT moreover showed that the particle displays an epitaxial relationship with the pyroxene (Fig. 5g).

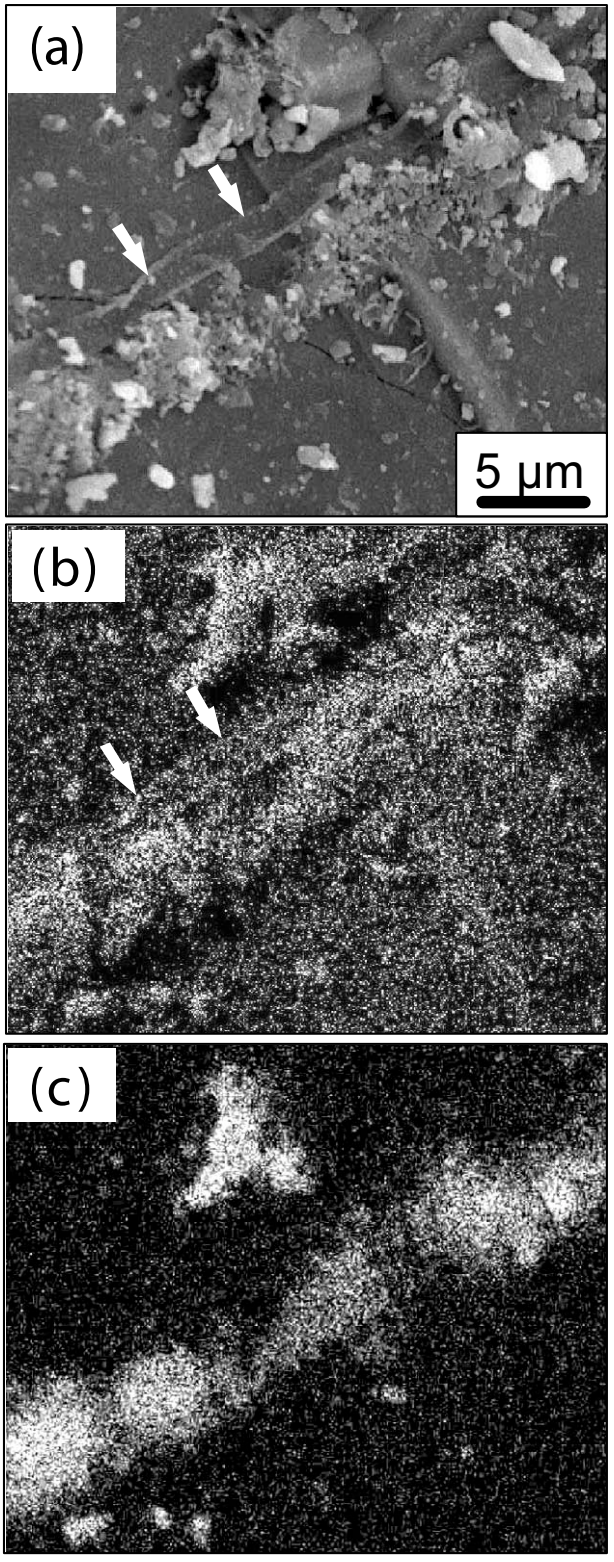

4. DISCUSSION

Two types of objects observed on the Tatahouine meteorite by SEM could *a priori* fulfill generally accepted biogenicity criteria (Westall, 1999): (1) the long flat filament which displays a microorganism-like morphology, and (2) the nannobacteria-like rods, which have recently been shown to be nanometer-sized calcite single crystals with a surrounding amorphous calcium carbonate layer (Benzerara et al., 2003).

4.1. Nature of the Filament

Recent debates have shown that the biologic origin of a single fossilized object is difficult to be unambiguously assessed (Garcia-Ruiz et al., 2003; Brasier et al., 2002). In this study, the filament, shown to consist mostly of carbon by SEM-EDXS, also contains oxygen, nitrogen, and phosphorus. Moreover, the carbon K-edge EELS spectra on it are typical of organic carbon species (Mansot et al., 2003). Morphology cannot be a criterion of biogenicity by itself (Benzerara et al., 2003; Cady et al., 2003), but it can be noticed that this filament has a well-defined shape, is 1 micron wide and tens of microns long, and that similar filaments have been observed several times on the Tatahouine meteorite fragments. Potential uncertainties regarding the origin of the filament may exist, but we believe that an organized structure displaying the shape and the expected size of a microorganism, composed of organic molecules and containing phosphorus and nitrogen, in a sample where it is expected to find abundant microbial life, is very likely a microorganism. Hence, in the following, we refer to this filament as a microorganism. Still, morphology is of little use to clarify the taxonomy of this filament, which could be either (1) a prokaryote: either belonging to *Actinomycetes* or *Cyanobacteria* groups as a large diversity of these taxons has been identified by 16S rRNA gene analyses of the Tatahouine meteorite fragments, or (2) a fungus (see Steele et al., 2000 for a similar discussion). The use of specific fluorescent nucleic probes of these taxonomic groups on the Tatahouine pyroxene crystals would be of great interest to address this issue.

EDXS and EELS analyses moreover suggest that this microorganism is fossilizing as shown by the enrichment in calcium and iron. The absence of iron-oxide or calcium carbonate nanocrystallites suggests either an adsorption of Fe and Ca to reactive groups of the microorganism, or more likely, given the relatively high concentration of these elements, the precipitation in the microorganism of small or amorphous clusters not detected during our TEM investigation. Amorphous carbonates and iron oxides are suspected because they are common during biomineralization (Chan et al., 2004; Aizenberg et al., 2002). The sources of the

Fig. 2. SEM observation and chemical mapping of a Tatahouine meteorite fragment collected in 2000. See Benzerara et al. (2003) for additional pictures of the same area. (a) The pyroxene (gray background) is colonized by a long and flat filament (arrows), which is bordered by a cluster of nanometer-sized calcite crystals (white area bottom side of the filament). (b) Carbon map. White areas correspond to higher concentration of carbon. The cluster and the filament (arrows) contain carbon. (c) Calcium map. Only the cluster can be observed, confirming that it is formed by calcium carbonate clusters as demonstrated by Benzerara et al. (2003).

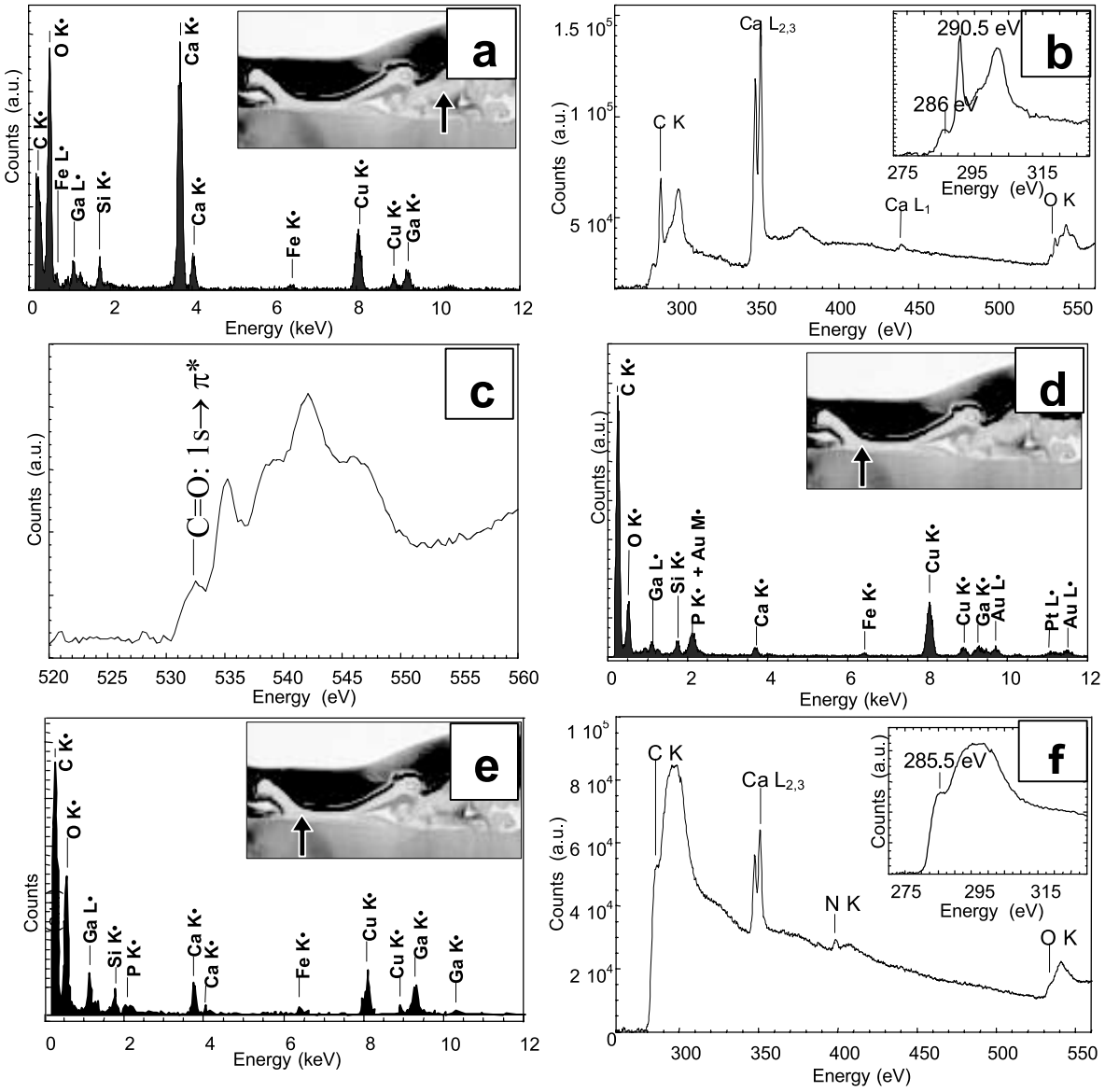

Fig. 3. (a) EDXS analysis on a calcite crystal. Note the presence of iron. (b) EELS analysis on the calcite crystals. The C-K edge is typical of carbon in carbonate groups. Insert: detail on the C-K edge showing a peak at 286 eV, which can be related either to the formvar of the TEM grid or to the sample. (c) O-K-edge EELS spectrum of the Tatahouine calcites. The peak at 532 eV is not related to the carbonate bond but could be indicative of carbonyl or carboxyl groups. This peak was not observed on the formvar film. (d) EDXS analysis on the microorganism. The copper signal comes from the grid. Gold was deposited before SEM observations. Platinum was deposited before the FIB milling procedure (see Experimental section). Mα emission line (2050 eV) overlaps the phosphorus Kα line (2013 eV). (e) EDXS analysis on a different area in the microorganism. We chose this area because the platinum Lβ emission line is not observed, in contrast to analysis (d). The peak at around 2010 eV can thus be indexed as phosphorus. (f) EELS analysis on the microorganism. Insert: detail on the C-K edge, which is typical of amorphous (here likely organic) carbon. Note the presence of nitrogen and calcium.

calcium and iron observed within the microorganism can be discussed. Because the orthopyroxene contains a low calcium concentration, calcium likely originates from the surrounding Tatahouine sand, which contains large quantities of calcium carbonates originating from the underlying bedrock (Barrat et al., 1999). Iron has likely been supplied to the microorganism under a soluble form, because no iron oxide crystallite was evidenced on the microorganism. Observation of dissolution features (i.e., the high roughness of the pyroxene surface beneath the microorganism) in the pyroxene below the microbe suggests that iron may come from the pyroxene (see below). A direct implication would be that the microorganism was present before or at least during the dissolution process, as discussed in section 4.3.

4.2. Origin of the Calcites

The observations made in this study confirm that the rod-shaped calcite crystals have carbonate carbon K-edge EELS

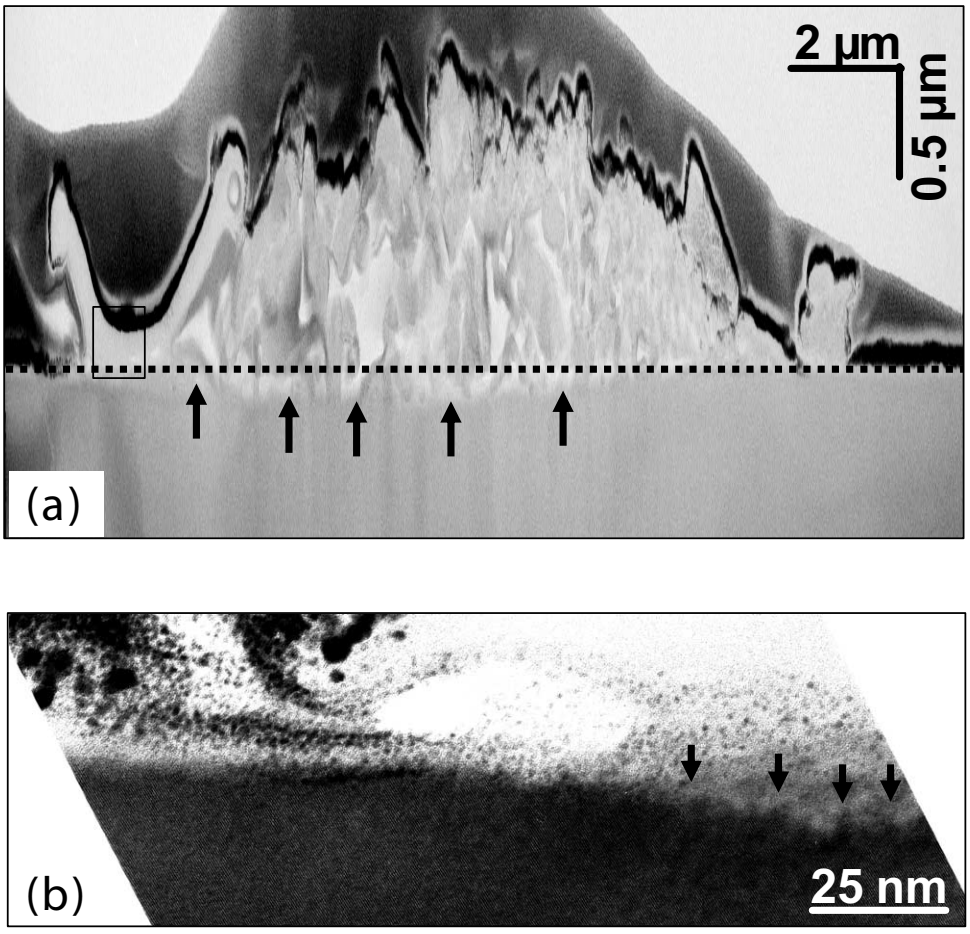

Fig. 4. TEM observation of the interface between the microorganism and the pyroxene. (a) The dotted line shows the horizontal surface of the pyroxene as observed on both sides of the cross-section. A 100-nm deep pit is obvious on this image (see arrows indicating the surface of the pyroxene) and is centered on the calcite cluster. Note the vertical stretching to highlight the pit. (b) High-resolution image of the area at the far left-hand side of the microorganism. The surface of the pyroxene directly in contact with the microorganism (right-hand side, see arrows indicating the area where the microorganism is in contact with the pyroxene) is rougher, suggesting a nano-pitting of the surface at this location. The surface not in direct contact with the microorganism (left-hand side of the image) is smoother.

spectra. Benzerara et al. (2003) observed that the formation of the nanometer-sized calcite crystals spatially correlates with the filament microorganism. In addition, the morphology of these calcite crystals and the presence of an amorphous calcium carbonate layer surrounding the crystals suggest a biogenic origin as proposed by Benzerara et al. (2003). C-K-edge EELS spectroscopy on the calcites shows the presence of a peak at 286 eV (Fig. 3), which results from the presence of noncarbonate carbon, but the use of a carbon film TEM grid prevents any conclusion. However, O-K edge EELS spectroscopy revealed the presence of a peak at 532 eV that is related neither to carbonate nor to the TEM grid (Hofer and Golob, 1987). According to Urquhart and Ade (2002) and Flynn et al. (2003), this peak may result from O 1s to π^* transitions in carbonyl or carboxyl groups. A higher spectral resolution would be useful to identify unambiguously those components. The existence of carbonyl or carboxyl groups associated with the calcite nanocrystals could be related to the presence of organic molecules released by the microorganism, forming a microenvironment responsible for the unusual morphology and structure of the observed calcite crystals (Aizenberg et al., 1999; Cölfen and Qi, 2001; Donners et al., 2002).

4.3. Implications for Microbial Pyroxene Weathering

The depression below the calcite cluster was evidenced all along the microbial filament by Benzerara et al. (2003). We did not observe similar 4-μm-wide, tens of μm long, and 100-nm-deep depressions on the meteorite fragments collected the day after the fall, neither did previous studies (Barrat et al., 1998). This depression at the surface of a pyroxene single-crystal is thus likely the result of dissolution. The co-location of the trench in the pyroxene surface with the filamentous microorganism suggests that dissolution of the orthopyroxene was enhanced at the vicinity of the microorganism (see Fig. 4a). One could imagine that the microorganism colonized the pyroxene after the formation of the depression. However, this scenario seems improbable as it would require that the microorganism aligns itself along the depression via an unknown mechanism. Moreover, observation of amorphous iron oxides

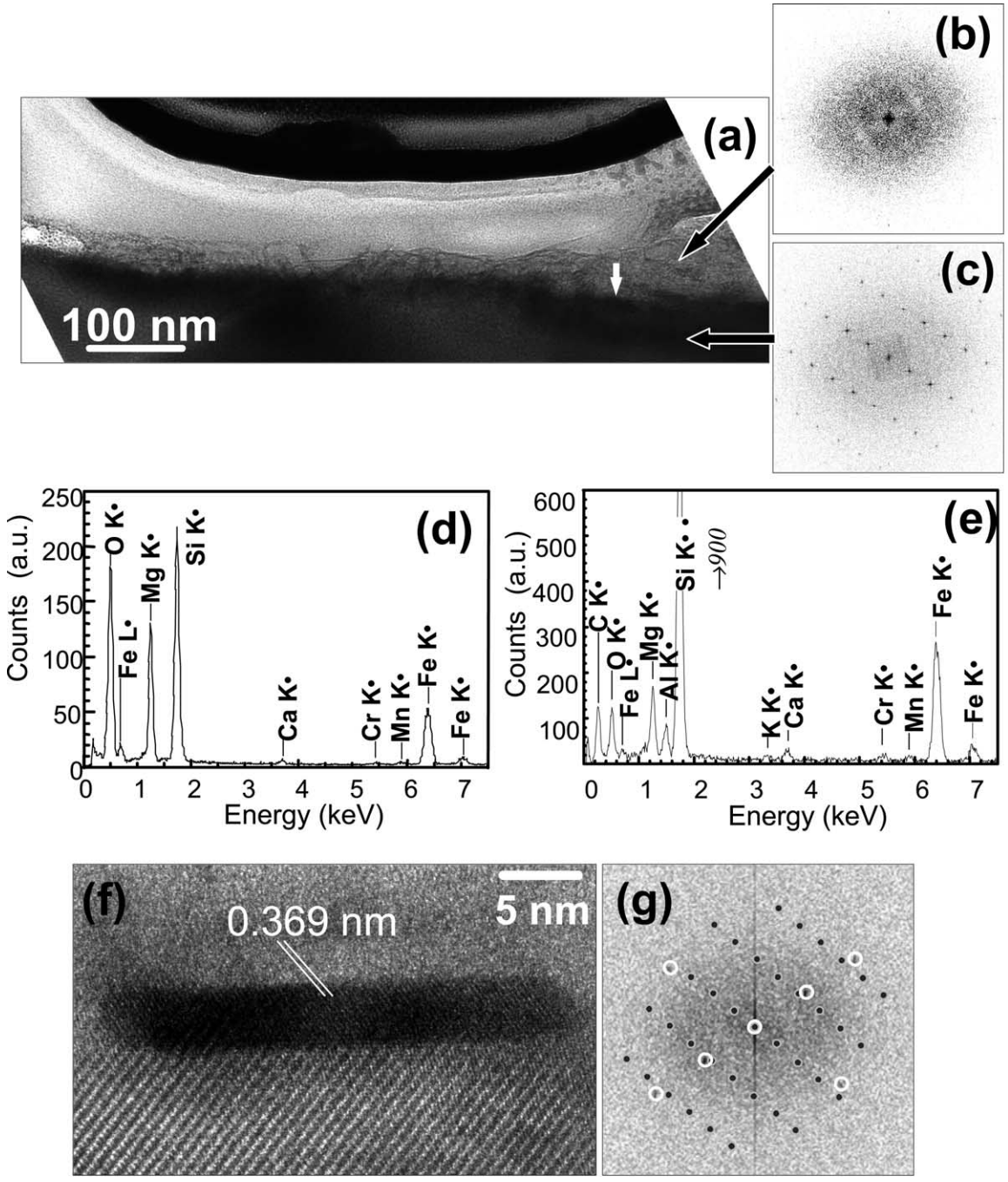

Fig. 5. (a) Image of the contact between the microorganism and the pyroxene (see rectangle in Fig. 4a). The image was defocused to enhance the contrast of noncoherently diffracting objects. A fibrous layer can be observed between the microorganism and the pyroxene. (b) Fast Fourier transform of a high-resolution image (see 5e around the rod-shaped particle) of the fibrous layer. No reflection can be seen, indicating that the layer is amorphous. (c) Fast Fourier transform of a high-resolution image (see 5e) taken in the pyroxene. (d) EDXS analysis on the pyroxene. (e) EDXS analysis on the fibrous layer between the microorganism and the pyroxene. This layer is depleted in Mg compared to the pyroxene, enriched in Al and Si, and contains K. (f) High-resolution image of a rod-shaped particle observed inside the aluminosilicate amorphous layer between the microorganism and the pyroxene (see arrow in 5a). (g) Fast Fourier transform of the particle. The diffraction pattern of the particle (circled spots) is superimposed with the pattern of the pyroxene (see 5c for the FFT of the pyroxene crystal alone) and shows a topotactical relationship with the pyroxene. The distances (3.69 and 2.15 Å) between the spots forming the two main directions on the diffraction pattern together with the angle (70°) between these two lines are consistent with (−112) and (−1–33) lattice planes of illite or smectite. EDXS analysis on the particle shows no significant difference with the surrounding aluminosilicate amorphous layer.

on the microorganism (see section 4.1) favors the hypothesis that the microorganism was already present when the dissolution occurred. Several experimental studies have proposed that microorganisms could enhance dissolution of silicates either by lowering pH locally, or by producing ion-complexing organic ligands, or via both processes (Banfield et al., 1999).

The observation that the microorganism is not located at the center of the trench, which instead is occupied by likely biogenic calcites (Benzerara et al. 2003) is somewhat puzzling. However, the microtopography of the pyroxene–microorganism interface (Fig. 4b) indicates that dissolution did occur below the microorganism and was, at least initially, surface-controlled. We observed the formation of an Al- and Si-rich amorphous layer exclusively below the microorganism. Based on BET measurements by Casey et al. (1989b), Hellmann et al. (2003) suggested that such layers are very porous and do not interfere with the dissolution rate of the minerals. However, Casey et al. (1989b) specified that the porosity appeared artifactually during drying and did not exist during the dissolution process. Moreover, we could not evidence any nanoporosity by HRTEM in our sample. Finally, even if the coating layer is porous, it may partially inhibit dissolution as explained by Nugent et al. (1998). Indeed, stagnant pore waters inside the coating may be more supersaturated with respect to pyroxene than the Tatahouine sand pore water, and thus the driving force for dissolution may be lowered. Thus, according to what has been proposed by numerous previous studies (e.g., White and Brantley, 2003; Nugent et al., 1998), the amorphous Al- and Si-rich layer observed on the Tatahouine + pyroxene beneath the microorganism could eventually inhibit further pyroxene dissolution. These rationales would explain why the depression is shallower below the microorganism compared to below aluminosilicate-free regions under the calcite cluster. Whereas many geomicrobiologic studies have stressed the enhancing effect of microorganisms on the dissolution of silicates, few have shown a lowering of mineral dissolution in the presence of attached microorganisms (Santelli et al., 2001; Benzerara et al., 2004; Lüttge and Conrad, 2004). In this study, we suggest that the presence of microorganisms can modify mineral dissolution rates in a more complex way with, in the same time, (1) the formation of coatings that passivate the surface beneath the microorganism and (2) an enhancement of dissolution close to the microorganism resulting from organic molecules released by the microorganism.

The question of stoichiometry is central for evaluating silicate alteration rates (Berner et al., 1985; Brantley and Chen, 1995). Quantitative study of natural weathering yields lower rates than those deduced in the laboratory (Brantley and Chen, 1995). Chemical affinity is a major parameter controlling dissolution rates, but it has been argued that the formation of an altered layer under some conditions could also partly explain this discrepancy (White and Brantley, 2003). Except for Nahon and Colin (1982), who did not actually provide a structural characterization at the nanometer scale, a residual amorphous layer has never been detected on naturally weathered pyroxene surfaces. Several previous investigators inferred nonstoichiometric weathering reactions at the lichen–mineral interface, but all employed procedures that destroyed textural information and drastically altered the mineralogical component, as noted by Barker et al. (1997). Using HRTEM, Barker and Banfield (1996) detected no leached layers or siliceous relicts on amphibole, feldspar, or biotite colonized by lichens. We show in this study that, at least under certain conditions, an amorphous residual layer can form. One question is whether this layer is (1) a leached layer resulting from preferential cation leaching or (2) a secondary layer resulting from a dissolution-reprecipitation process. The answer is beyond the scope of this study as the chemical conditions prevailing during the weathering of this natural sample are not precisely known. However, it can be noted that similarly to Hellmann et al. (2003) who favor the second hypothesis, we observed a very sharp structural transition between the crystallized pyroxene and the amorphous aluminosilicate layer with no amorphous island below the interface and no remnant pyroxene crystallites above the interface. The ability of some microorganisms to promote aluminosilicate precipitation (e.g., Kawano and Tomita, 2002) could be a mechanism involved in the preferential formation of the amorphous layer beneath the filament. Casey et al. (1993) have hypothesized the existence of gel-like layers at the surface of weathered pyroxenes to explain the topotactic growth of phyllosilicates on these minerals. This scheme is supported by our observation of a nanometer-sized clay particle in the amorphous layer growing in epitaxial relationship with the pyroxene (Fig. 5).

The fate of dissolved iron is intriguing. X-ray Photoelectron Spectroscopy (XPS) measurements by Schott and Berner (1983) on bronzite dissolved under oxic conditions at pH 6 showed the formation of a tens of Å thick hydrous ferric oxide and Fe^{3+} hydroxylated silicate precipitate which may passivate the pyroxene surface and lower subsequent dissolution (see also Casey et al., 1993). We could not detect any oxy(hydroxy) iron precipitate at the pyroxene surface. In this view, our observations would be more consistent with Schott and Berner's (1983) study of bronzite dissolution under anoxic conditions where no such layer was detected. Such conditions would however be unexpected at the very near surface of the Tatahouine sand.

Rough mass balance estimations of the calcium released by orthopyroxene dissolution and trapped by calcite precipitation indicate that most of the calcite calcium comes from the surrounding Tatahouine soil. However, an important issue is deciphering whether cations released by pyroxene dissolution are trapped in calcite crystals or not. This trapping would mean that the calcite formation occurs simultaneously with pyroxene dissolution and that a Urey-type CO_2 sequestration mechanism is operating (Urey, 1952). EDXS peaks showed the presence of iron and magnesium in some calcite grains in the sample studied here, as well as in samples collected at the surface of the meteorite by micromanipulation (data not shown). Magnesium and iron could potentially come from the surrounding environment. However, as the pH in the Tatahouine sand is likely buffered by carbonates, the solubility of iron is likely low. Thus, we suggest that magnesium and iron come from the dissolution of the iron- and magnesium-rich Tatahouine pyroxene, occurring just below the calcite precipitation. The scenario proposed here seems to be the simplest one consistent with the observations; it may, however, not be the only one. The trace element composition of the Tatahouine meteorite is unique (Barrat et al., 1999). A spatially resolved analytical technique capable of measuring trace element concentrations would pos-

sibly assist in tracking a potential pyroxene source in the calcite trace element composition.

5. CONCLUSION

The focused ion beam technique has been developed in the semiconductor and nanotechnology industries (Giannuzzi and Stevie, 1999). The present study shows that the focused ion beam technique also offers great promise in the study of microbe–mineral interactions. The coupling with analytical TEM allows identification of organic and mineral materials and their structural and chemical relationship at the nanometer scale. This study elucidated how a not yet taxonomically classified microorganism impacts pyroxene weathering and how adjacent calcite nanocrystals are likely associated with the microorganism. It sheds new light on the complex control of microorganisms on silicate weathering. Amorphous layers formed during pyroxene weathering, whose natural existence is debated, are shown here to be associated with the microorganism.

Acknowledgments—The French Ministry of Foreign Affairs partly funded Karim Benzerara's postdoctoral position by the Lavoisier program. We thank Jean-Alix Barrat who initiated the whole work on the weathering of the Tatahouine meteorite. We thank Aaron Slowey for helpful corrections on the English language and style, and Christian Dominici for SEM analyses. We thank Liane G. Benning, Mihály Pósfai, and an anonymous reviewer for detailed and constructive critiques of an early version of this work.

Associate editor: L. Benning

REFERENCES

Aizenberg J., Black A. J., and Whitesides G. H. (1999) Oriented growth of calcite controlled by self-assembled monolayers of functionalized alkanethiols supported on gold and silver. *J. Am. Chem. Soc.* **121,** 4500–4509.

Aizenberg J., Lambert G., Weiner S., and Addadi L. (2002) Factors involved in the formation of amorphous and crystalline calcium carbonate: A study of an ascidian skeleton. *J. Am. Chem. Soc.* **124,** 32–39.

Banfield J. F., Ferruzzi G. G., Casey W. H., and Westrich H. R. (1995) HRTEM study comparing naturally and experimentally weathered pyroxenoids. *Geochim. Cosmochim. Acta* **59,** 19–31.

Banfield J. F., Barker W. W., Welch S. A., and Taunton A. (1999) Biological impact on mineral dissolution: Application of the lichen model to understanding mineral weathering in the rhizosphere. *Proc. Natl. Acad. Sci. USA* **96,** 3404–3411.

Barker W. W. and Banfield J. F. (1996) Biologically versus inorganically mediated weathering reactions: Relationships between minerals and extracellular microbial polymers in lithobiontic communities. *Chem. Geol.* **132,** 55–69.

Barker W. W., Welch S. A., and Banfield J. F. (1997) Biogeochemical weathering of silicate minerals. *Rev. Mineral.* **35,** 391–428.

Barrat J. A., Gillet P., Lecuyer C., Sheppard S. M. F., and Lesourd M. (1998) Formation of carbonates in the Tatahouine meteorite. *Science* **280,** 412–414.

Barrat J. A., Gillet P., Lesourd M., Blichert-Toft J., and Poupeau G. R. (1999) The Tatahouine diogenite: Mineralogical and chemical effects of sixty-three years of terrestrial residence. *Meteorit. Planet. Sci.* **34,** 91–97.

Benzerara K., Menguy N., Guyot F., Dominici C., and Gillet P. (2003) Nanobacteria-like calcite single crystals at the surface of the Tataouine meteorite. *Proc. Natl. Acad. Sci. USA* **100,** 7438–7442.

Benzerara K., Barakat M., Menguy N., Guyot F., De Luca G., Audrain C., and Heulin T. (2004) Experimental colonization and alteration of orthopyroxene by the pleomorphic bacteria *Ramlibacter tataouinensis. Geomicrob. J.* **21,** 341–349.

Berner R. A. (1995) Chem. weathering and its effect on atmospheric CO_2 and climate. *Rev. Mineral.* **31,** 565–583.

Berner R. A., Holdren G. R., and Schott J. (1985) Surface-layers on dissolving silicates, comment. *Geochim. Cosmochim Acta* **49,** 1657–1658.

Brantley S. L. and Chen Y. (1995) Chemical weathering rates of pyroxenes and amphiboles. *Rev. Mineral.* **31,** 119–172.

Brasier M. D., Green O. R., Jephcoat A. P., Kleppe A. K., Van Kranendonk M. J., Lindsay J. F., Steele A., and Grassineau N. V. (2002) Questioning the evidence for Earth's oldest fossils. *Nature* **416,** 76–81.

Cady S. L., Farmer J. D., Grotzinger J. P., Schopf J. W., and Steele A. (2003) Morphological biosignatures and the search for life on Mars. *Astrobiology* **3,** 351–368.

Casey W. H., Westrich H. R., Arnold G. W., and Banfield J. F. (1989a) The surface-chemistry of dissolving labradorite feldspar. *Geochim. Cosmochim. Acta* **53,** 821–832.

Casey W. H., Westrich H. R., Massis T., Banfield J. F., and Arnold G. W. (1989b) The surface of labradorite feldspar after acid-hydrolysis. *Chem. Geol.* **78,** 205–218.

Casey W. H., Westrich H. R., Banfield J. F., Ferruzzi G., and Arnold G. W. (1993) Leaching and reconstruction at the surfaces of dissolving chain-silicate minerals. *Nature* **366,** 253–256.

Chan C. S., De Stasio G., Welch S. A., Girasole M., Frazer B. H., Nesterova M. V., Fakra S., and Banfield J. F. (2004) Microbial polysaccharides template assembly of nanocrystal fibers. *Science* **303,** 1656–1658.

Cölfen H. and Qi L. M. (2001) A systematic examination of the morphogenesis of calcium carbonate in the presence of a double-hydrophilic block copolymer. *Chem. Eur. J.* **7,** 106–116.

Donners J. J. J. M., Nolte R. J. M., and Sommerdijk N. A. J. M. (2002) A shape-persistent polymeric crystallization template for $CaCO_3$. *J. Am. Chem. Soc.* **124,** 9700–9701.

Flynn G. J., Keller L. P., Feser M., Wirick S., and Jacobsen C. (2003) The origin of organic matter in the solar system: Evidence from the interplanetary dust particles. *Geochim. Cosmochim. Acta* **67,** 4791–4806.

Garcia-Ruiz J. M., Hyde S. T., Carnerup A. M., Christy A. G., Van Kranendonk M. J., and Welham N. J. (2003) Self-assembled silica-carbonate structures and detection of ancient microfossils. *Science* **302,** 1194–1197.

Giannuzzi L. A. and Stevie F. A. (1999) A review of focused ion beam milling techniques for TEM specimen preparation. *Micron* **30,** 197–204.

Heaney P. J., Vicenzi E. P., Giannuzzi L. A., and Livi K. J. T. (2001) Focused ion beam milling: A method of site-specific sample extraction for microanalysis of Earth and planetary materials. *Am. Min.* **86,** 1094–1099.

Hellmann R., Penisson J. M., Hervig R. L., Thomassin J. H., and Abrioux M. F. (2003) An EFTEM/HRTEM high-resolution study of the near surface of labradorite feldspar altered at acid pH: Evidence for interfacial dissolution-reprecipitation. *Phys. Chem. Min.* **30,** 192–197.

Hofer F. and Golob P. (1987) New examples for near-edge fine structures in electron energy loss spectroscopy. *Ultramicroscopy* **21,** 379–383.

Kawano M. and Tomita K. (2002) Microbiotic formation of silicate minerals in the weathering environment of a pyroclastic deposit. *Clays and Clay Min.* **50,** 99–110.

Lacroix A. (1932) La météorite (diogénite) de Tataouine, Tunisie (27 Juin 1931). *Bulletin de la Société Française de Minéralogie* **55,** 101–122.

Lüttge A. and Conrad P. G. (2004) Direct observation of microbial inhibition of calcite dissolution. *Appl. Environ. Microbiol.* **70,** 1627–1632.

Mansot J. L., Golabkan V., Romana L., and Cesaire T. (2003) Chemical and physical characterization by EELS of strontium hexanoate reverse micelles and strontium carbonate nanophase produced during tribological experiments. *J. Microsc.* **210,** 110–118.

Nahon D. B. and Colin F. (1982) Chemical weathering of orthopyroxenes under lateritic conditions. *Am. J. Sci* **282,** 1232–1243.

Nesbitt H. W. and Muir I. J. (1988) SIMS depth profiles of weathered plagioclase and processes affecting dissolved Al and Si in some acidic soil solutions. *Nature* **334,** 336–338.

Nugent M. A., Brantley S. L., Pantano C. G., and Maurice P. A. (1998) The influence of natural mineral coatings on feldspar weathering. *Nature* **395,** 588–591.

Oelkers E. H. and Schott J. (2001) An experimental study of enstatite dissolution rates as a function of pH, temperature, and aqueous Mg and Si concentration and the mechanism of pyroxene/pyroxenoid dissolution. *Geochim. Cosmochim. Acta* **65,** 1219–1231.

Santelli C. M., Welch S. A., Westrich H. R., and Banfield J. F. (2001) The effect of Fe-oxidizing bacteria on Fe-silicate mineral dissolution. *Chem. Geol.* **180,** 99–115.

Schott J. and Berner R. A. (1983) X-ray photoelectron studies of the mechanism of iron silicate dissolution during weathering. *Geochim. Cosmochim. Acta* **47,** 2233–2240.

Steele A., Goddard D. T., Stapleton D., Toporski J. K. W., Peters V., Bassinger V., Sharples G., Wynn-Williams D. D., and McKay D. S. (2000) Investigations into an unknown organism on the Martian meteorite Allan Hills 84001. *Meteor. Planet. Sci.* **35,** 237–241.

Urey H. C. (1952) *The Planets, Their Origin and Development.* Yale Univ. Press, New Haven.

Urquhart S. G. and Ade H. (2002) Trends in carbonyl core (C 1s, O1s) $\pi^*C=0$ Transition in the near-edge X-ray absorption structure spectra of organic molecules. *J. Phys. Chem. B* **106,** 8531–8538.

Westall F. (1999) The nature of fossil bacteria: A guide to the search for extraterrestrial life. *J. Geophys. Res. Planets* **104,** 16437–16451.

White A. F. and Brantley S. L. (2003) The effect of time on the weathering of silicate minerals: why do weathering rates differ in the laboratory and field? *Chem. Geol.* **202,** 479–506.